Journal of Catalysis 267 (2009) 24–29

Contents lists available at ScienceDirect

Journal of Catalysis

journal homepage: www.elsevier.com/locate/jcat

Meso- and nano-structuring of industrial Cu/ZnO/(Al_2O_3) catalysts

Malte Behrens *

Fritz-Haber-Institute of the Max-Planck-Society, Inorganic Chemistry Department, Faradayweg 4-6, 14195 Berlin, Germany

ARTICLE INFO

Article history:
Received 4 June 2009
Revised 17 July 2009
Accepted 19 July 2009
Available online 22 August 2009

Keywords:
Cu/ZnO
Nanostructured catalysts
Methanol synthesis
Catalyst preparation
Precursor chemistry

ABSTRACT

A concept is presented, which helps to rationalize the success of the industrially applied preparation route for Cu/ZnO/(Al_2O_3) catalysts. Many studies can be found in the open literature, which describe the critical dependency of the final catalyst's properties on precursor chemistry. In line with previous reports, this concept identifies zincian malachite as the relevant precursor phase and includes a simple relation of precursor crystal structure and final Cu surface area. It comprises two hierarchical microstructure-directing effects, for which particle morphology and degree of Cu^{2+} substitution by Zn^{2+} in the zincian malachite phase are the key properties: (i) meso-structuring of the precursor phase upon ageing of the co-precipitate in the mother liquor and (ii) nano-structuring of the oxide phase upon decomposition. Consequences for further optimization of the Cu, Zn, Al system are discussed.

1. Introduction

The Cu/ZnO/Al_2O_3 catalyst system is of high industrial importance and employed, e.g. for the synthesis of methanol from H_2/CO_2/CO mixtures at low temperature and pressure (ca. 250 °C, 60 atm). The binary Cu/ZnO system serves as a model system for industrially applied catalysts, which usually contain 5–10 mol% Al_2O_3. A successful route of preparation leading to highly active catalysts was developed in the second half of the last century [1,2] and studied and optimized by many academic and industrial research groups ever since. This synthesis comprises co-precipitation at constant pH, ageing of the precipitate in the mother liquor and calcination after washing and drying. Finally, the catalyst is activated by reduction of the Cu oxide component. A large body of work reports on the complex dependencies of the catalyst's properties on the various parameters of the precipitation and ageing process [3–9] and this phenomenon is referred to as the chemical memory of the system [9]. The detailed work of Waller et al. [3] identified zincian malachite, $(Cu,Zn)_2(CO_3)(OH)_2$, as the relevant precursor phase, while other authors suggest that the presence of aurichalcite, $(Cu,Zn)_5(OH)_6(CO_3)_2$, is essential for the preparation of an active Cu/ZnO catalyst [10,11]. Indeed, most active catalysts were often found for Cu:Zn ratios, which lead to the formation of a phase mixture of zincian malachite and aurichalcite.

Although the preparation process can to some extent be regarded as optimized as a result of many mostly empirical studies, a clear and comprehensive model is not yet established, which explains the benefit of the technically applied process. The aim of this paper is to contribute to the understanding of the chemical memory by introducing a two-step model for the successful meso- and nano-structuring of Cu/ZnO/(Al_2O_3) catalysts, which relates their chemistry of precipitation and ageing in the course of the industrially applied preparation process with their unique catalytic properties. The model is discussed in the context of the work on this issue already published in the open literature.

2. Materials and methods

A series of Cu, Zn precursors with varying Cu:Zn ratio was prepared by constant-pH co-precipitation at pH 7 and $T = 65$ °C and the results were presented in an earlier contribution [9]. The precipitates were aged in the mother liquor for 2 h and recovered by filtration, washing and drying. Further details on the preparation process can be found in Ref. [9]. Cu/ZnO catalysts were prepared from these precursors by calcination (330 °C for 3 h) and reduction in diluted hydrogen at 250 °C. The decomposition behavior during calcination was simulated with thermogravimetric analysis (TGA) and it was found that all samples show their major mass loss step below 350 °C. However, a small fraction of residual carbonate was decomposed at temperatures between 380 and 500 °C and, thus, remains in the material upon calcination. A detailed discussion of the TGA results can be found in Ref. [9]. The reduction of Cu(II) to Cu(0) was completed at 250 °C for all samples with onset temperatures between 170 and 200 °C. The activated samples were structurally characterized and tested in methanol synthesis. The copper surface area was determined applying N_2O reactive frontal chromatography according to the method proposed by Chinchen

* Fax: +49 30 8413 4405.
E-mail address: behrens@fhi-berlin.mpg.de

0021-9517/$ - see front matter © 2009 Elsevier Inc. All rights reserved.
doi:10.1016/j.jcat.2009.07.009

et al. [12] at somewhat more moderate reaction conditions [13]. These results were reported in Ref. [14]. Herein, the structural properties of the precursors are related with the gas accessible Cu surface areas of the final Cu/ZnO catalysts.

To better understand this relation, the preparation of the precursor material with a Cu:Zn ratio of 70:30 was reproduced under similar conditions in an automated laboratory reactor (Mettler Toledo Labmax). For this experiment 500 ml of a 1 M Cu, Zn nitrate solution was dosed into a 400 ml-reservoir of bi-distilled water within 20 min while the pH was adjusted to 7 by simultaneous addition of appropriate amounts of a 1.2 M Na_2CO_3 solution. The temperature of the reactor was kept at 65 °C during co-precipitation and ageing. Aliquots (ca. 20 ml of suspension) were recovered after certain time intervals of ageing in the mother liquor. The solids were washed with distilled water and dried in air at 60 °C over night. A ternary $Cu/ZnO/Al_2O_3$ sample of the metal composition Cu:Zn:Al = 60:25:15 was prepared accordingly.

XRD patterns were recorded on a STOE Stadi-P diffractometer using Cu Kα radiation and a primary monochromator in transmission geometry. ICDD files 72-75 (malachite) and 17-743 (aurichalcite) were used for phase identification. SEM images were taken in a Hitachi S-4800 (FEG) system. HRTEM images were taken on a Philips CM200FEG microscope operated at 200 kV. The coefficient of spherical aberration was C_s = 1.35 mm. The information limit was better than 0.18 nm allowing the principal phases to be identified in HRTEM images. High-resolution images with a pixel size of 0.016 nm were taken at the magnification of 1,083,000× with a CCD camera. Specific surface areas were determined by N_2 physisorption in a Quantachrome Autosorb-1 machine. For measurement of hydrodynamic radii the washed solids (ca. 4 mg of wet filter cake) were re-dispersed in water (40 ml) and ultra-sonicated (100 W for 60 s). Large agglomerates were separated by centrifugation (5500 rpm for 5 min) and the dispersion was subjected to dynamic light scattering in a Malvern Zetasizer Nano ZS device.

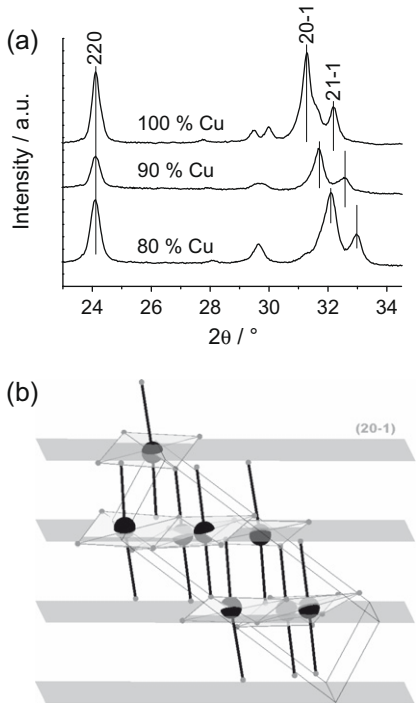

Fig. 1. Shift of the $20\bar{1}$ and $21\bar{1}$ reflections to higher angles as a function of Zn incorporation into malachite (a), arrangement of the CuO_6 octahedra in the malachite unit cell relative to the $(20\bar{1})$ netplanes, the Jahn–Teller elongated axes are drawn as thick black lines (b).

3. Results and discussion

We recently presented a study on the properties of single phase precursor materials, a binary Cu, Zn precursor phase mixture and mineral reference compounds [15]. As a result, the relation between distinct structural features of the zincian malachite precursor phase, $(Cu,Zn)_2(CO_3)(OH)_2$, – namely the *d*-spacing of the $20\bar{1}$ and $21\bar{1}$ reflections – and the Cu:Zn ratio was interpreted as a ligand field effect. In brief, the average Jahn–Teller distortions of the MO_6 octahedra in the malachite crystal structure are lowered as Cu^{2+} ions (d^9, Jahn–Teller distorted coordination preferred) are gradually substituted by Zn^{2+} (d^{10}, no Jahn–Teller distortion). This effect results in a pronounced shift of the above-mentioned reflections to lower *d*-spacings as a function of nominal composition (Fig. 1a), because all Jahn–Teller elongated axes of the eight CuO_6 octahedra in malachite unit cell are orientated nearly perpendicular to either one of these sets of netplanes. This is shown in Fig. 1b for the $(20\bar{1})$ planes, which correspond to the stronger XRD line. The position on the angular scale of most of the other reflections remains more of less constant.

It is well established that the optimal and industrially applied Cu:Zn ratio is between 2 and 3 and it was already mentioned in Ref. [15] that this represents the regime of highest Zn incorporation in the malachite phase achievable for the conditions used in Ref. [9]. For these precursors, an upper limit for the Zn occupancy of the metal sites in zincian malachite of 28% was estimated, resulting in a Cu:Zn ratio of ca. 2.6 for this special precursor phase. In Fig. 2 the $d(20\bar{1})$ spacing of the (zincian) malachite precursor phase and the Cu surface area of the resulting Cu/ZnO catalyst are shown as function of composition. It can be seen that the Cu surface area has a maximum near this critical Zn content. This observation supports the idea that a highly Zn-substituted form of zincian malachite is the relevant precursor phase for the preparation of Cu/ZnO catalysts with large Cu surface areas. The Cu:Zn ratio should be chosen such that the limit of Zn incorporation (28% for the conditions used for this study) is targeted.

It has to be mentioned that the methanol synthesis activities also shown in Fig. 2 and reported in Ref. [14] do not correlate with the Cu surface areas cited in Fig. 2 in a strictly linear fashion, but show some deviation. However, a large Cu surface area is generally accepted as a prerequisite for highly active $Cu/ZnO/(Al_2O_3)$ catalysts and can be seen as a major goal of catalyst preparation. A discussion on the influence of additional intrinsic factors on the activity of the samples under consideration, such as Cu lattice strain, can be found in detail in Ref. [14]. It is interesting to note that the reverse water gas shift activities reported by Stone and Waller [16] as a function of Cu:Zn ratio follow a trend, which is very similar to the evolution of Cu surface areas observed for our samples shown in Fig. 2. While it is nowadays widely accepted that Cu(0) carries the active sites for methanol synthesis, the nature of the active centers is still under debate. Especially, the role of ZnO is of importance and seems to go beyond the function as physical support or geometrical spacer. Strong metal support interactions are discussed to contribute to the so-called synergy in the Cu/ZnO system [17,18]. A general model of the Cu–ZnO interactions and their dynamics was elaborated by the Topsøe group [19,20], which was included in a microkinetic model [21] and has been recently enhanced [22]. They observed reversible changes in Cu particle morphology and decoration with ZnO entities as an answer to the reductive potential of the gas atmosphere for Cu/ZnO model catalysts of low loading. For industrial samples – those prepared via the zincian malachite precursor – also the presence of defects and structural disorder is discussed to contribute to the specific activity of the Cu(0) surface [23].

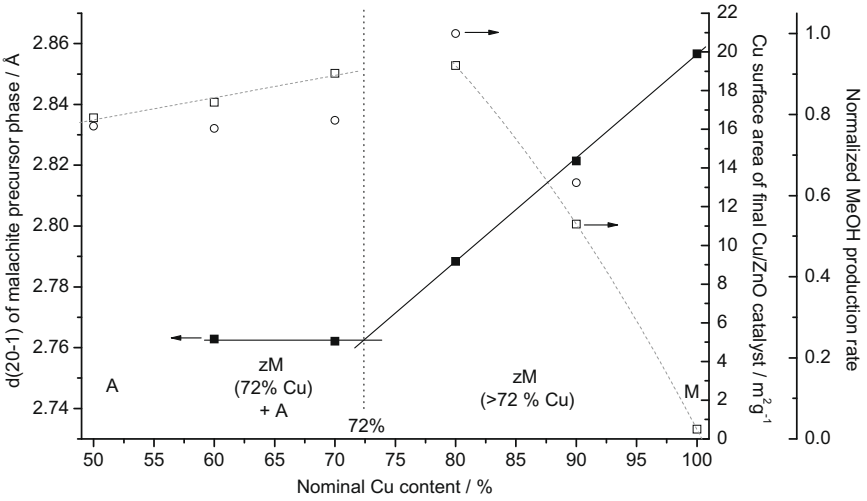

Fig. 2. d-Spacing of the $20\bar{1}$ netplanes of the zincian malachite precursor phase (solid squares), Cu surface area (open squares) and normalized methanol production rates (spheres) of the final binary model catalyst as a function of nominal Cu content. Presence of the phases aurichalcite (A), zincian malachite (zM) and malachite (M) is indicated.

The mixed cationic sub-lattice of the zincian malachite precursor phase is evidenced by the trend of the $d(20\bar{1})$ spacing shown in Fig. 2 and represents a perfect distribution of both elements on an atomic level. The monoxides Tenorite, CuO, and Zincite, ZnO, are – due to their different crystal structure – only very poorly dissolvable into each other. Hence, upon thermal decomposition of the precursor, individual nano-particles of CuO and ZnO will be formed [5]. A detailed TEM study of this particle formation process by calcination of Cu, Zn, Al precursor crystallites was recently presented by Baltes et al. [7]. The benefit of a high substitution level of the precursor phase is obvious, since the resulting oxide particles will be smaller and better intermixed the more homogeneous the initial distribution of Cu^{2+} and Zn^{2+} in the precursor is. Thereby, a distribution within the common cationic sub-lattice of a single phase will be much more effective than the intermixing of individual Cu-rich and Zn-rich precursor phases, displaying a distribution on a microscopic, but not on an atomic level. The resulting mixture of small CuO and ZnO particles maintains its nano-structured form upon reduction. TEM images of a reduced Cu/ZnO catalyst, which was prepared from the precursor with a Cu:Zn ratio of 70:30, i.e. from a fully substituted zincian malachite, are shown in Fig. 3. Cu and ZnO nanoparticles are arranged in an alternating fashion to form larger porous aggregates. This kind of microstructure explains the high Cu surface area observed for this special precursor composition.

It can be seen from Fig. 2 that for Cu-rich zincian malachite precursors the Cu surface area dramatically breaks down as the Cu content is increased well above 72%. In a microscopic picture, the CuO particles formed by decomposition of these samples will be much larger than the ZnO particles due to the deficit of Zn^{2+} in the precursor phase. Consequently, the dispersion of Cu will be poorer. The non-linearity of the curve can be explained with a Cu-loading effect, which is superimposed onto the dispersion effect. On the other side of the maximum the critical Zn concentration is exceeded and aurichalcite is formed as a Cu-poorer by-phase for Cu contents well below 72%. The fully substituted zincian malachite phase co-exists with aurichalcite for Cu contents between 72 and ca. 60%, but the decreasing amount of the former phase leads to a drop of Cu surface area as the nominal Cu content is lowered. The detrimental effect of aurichalcite formation, i.e. if the Cu:Zn ratio was chosen too low, is less pronounced compared to the detrimental effect of a Cu:Zn ratio, which is too high, as can be seen from the different slopes of the Cu surface area curve on either side of the maximum (Fig. 2). Therefore, in practical preparations it is wise to approach the maximum of Zn incorporation into malachite (and of Cu surface area in the final Cu/ZnO catalyst) from the high Zn-content side. Indeed, the industrially applied composition is usually close to 70:30, i.e. just in the regime, where aurichalcite starts to form as a by-phase. In this picture, the presence of just a little bit of aurichalcite – it is around 5 wt.% for Cu:Zn = 70:30 under the above-mentioned conditions [15] – can be seen rather as an indicator that the maximum substitution of zinican malachite was just exceeded than as an important or kind of synergetic precursor phase, whose presence is necessary for the final catalyst.

Still, this model does not explain the intrinsically lower Cu surface areas of catalysts prepared from aurichalcite precursors compared to ex-zincian malachite samples. According to the above considerations, the decomposition of a mixed precursor phase should yield the smallest CuO and ZnO particles for a 1:1 mixture of Cu^{2+} and Zn^{2+} in the common cation lattice of the precursor. It can be roughly estimated that due to the high dispersion of CuO (and ZnO) after calcination such samples should also result in the largest Cu surface areas after reduction. However, at 50% Zn, where a pure aurichalcite precursor is present [9], the measured Cu surface area is significantly lower compared to the critical Zn content for the zincian malachite phase of around 28% (Fig. 2).

It is proposed that another upstream microstructure-directing effect is responsible for the intrinsically higher Cu surface areas of the samples prepared from the fully substituted zincian malachite precursor. A likely explanation can be found in the unique chemistry of ageing of the malachite precursor. A precipitation and ageing log for the preparation of a CuZn precursor (Cu:Zn = 70:30) is shown in Fig. 4a. Co-precipitation is performed at constant pH by simultaneous dosing of metal solution and precipitating agent ($t_{ageing} < 0$ in Fig. 4a). Upon co-precipitation, first an amorphous precipitate is formed, which is transformed into the crystalline precursor during the ageing period in the mother liquor, typically after a few hours [3,8,9]. This crystallization is accompanied by a minimum in pH, an increase on turbidity and a change of color from blue to bluish green (after 65 min in Fig. 4a). This kind of behavior was only observed for Cu-rich compositions, i.e. in the compositional regime of zincian malachite [9]. As revealed by dynamic light scattering, electron microscopy and nitrogen adsorption measurements shown in Fig. 4 for samples, which were recovered from the precipitate slurry before and after

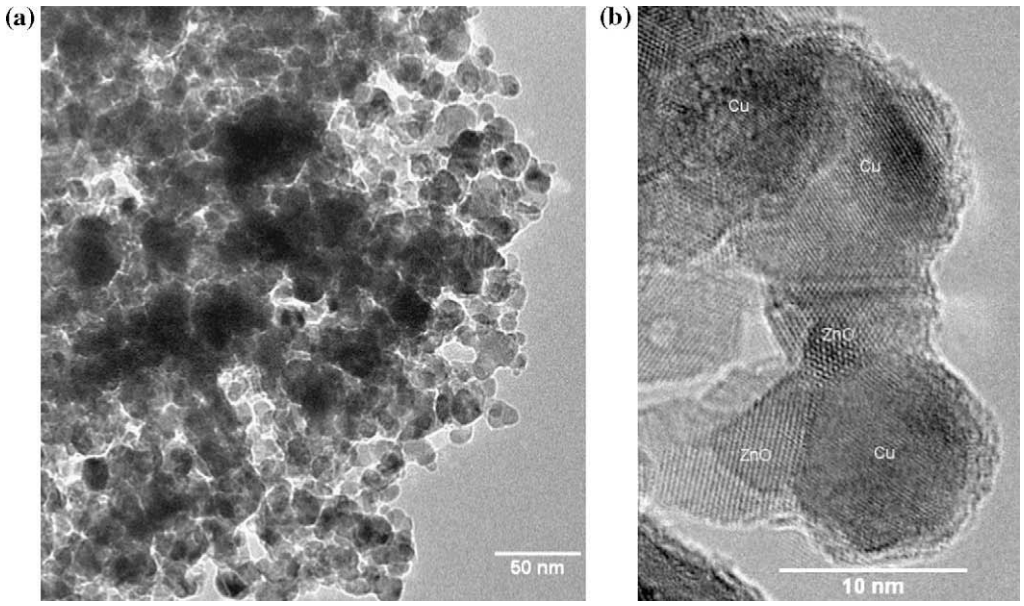

Fig. 3. TEM images showing the reduced binary Cu/ZnO catalyst prepared from a precursor with a Cu:Zn ratio of 70:30.

the crystallization, also the particle size, morphology and surface area of the precursor are affected during the ageing period. These observations are well in line with the results reported by Whittle et al. [5] on the effect of precipitate ageing on particle morphology for a precursor of the Cu:Zn ratio of 2:1. Initially, amorphous particles of undefined shape are present directly after co-precipitation. Upon ageing, they are transformed most probably by dissolution and re-precipitation events into small crystalline needles of zincian malachite (Fig. 4d and e). For the zincian malchite fraction in our binary model precursor (Cu:Zn = 70:30) shown in Fig. 4, these needles measure ca. 30 × 100 nm and are arranged in a loose network. Their formation is accompanied by a considerable increase of the specific surface area. Small amounts of aurichalcite are also formed as can be seen in the XRD pattern of the precursor after ageing. Aurichalcite crystallites are reported to exhibit a considerably more bulky and platelet-like morphology [3]. Thus, the resulting Cu particles may be smaller in ex-aurichacite samples due to a Cu:Zn ratio closer to unity, but they will be embedded in bulky aggregates due to the unfavorable meso-structure of the aurichalcite precursor phase. Their accessibility to the reactant gas phase will be significantly lower explaining the lower Cu surface area for sample prepared from a pure aurichalcite precursor despite the favorable Cu:Zn ratio of 1:1 as seen in Fig. 2.

Delayed crystallization during ageing seems to be unique to the malachite system and an amorphous form of zincian malachite, "zincian georgeite" $(Cu,Zn)(CO_3)(OH)_2$, was identified as the initial product of co-precipitation [24]. This step of ageing is all-important, not only for the phase formation, but also for the development of the unique meso-structure of the catalyst. Accordingly, ageing was reported to be essential for highly active catalysts by many authors [3,5,24,25].

According to the model described above, the benefit of the industrial preparation process is due to a hierarchical two-step microstructure-directing process, which is unique for the zinican malachite phase. Electron microscopy images of the relevant stages of catalyst preparation (meso-structuring during ageing, nano-structuring during calcination and finally activation by reduction) are shown in Fig. 5 for a ternary sample of the industrially relevant metal composition of Cu:Zn:Al = 60:25:15. The zincian malachite precursor phase is also present in such ternary systems, but an obvious difference to the binary system is that due to the presence of Al^{3+} not aurichalcite, but usually a hydrotalcite-like compound is formed as a Cu-poorer indicator phase, which forms as the nominal Zn content is increased above the critical limit.

First, the relatively large and bulky particles of the initial precipitate (Fig. 5a) transform into a loose network of zincian malachite needles during ageing. The particle size is lowered from the low μm scale for the initial precipitate to a few tens of nanometers for the thin dimension of the needles (Fig. 5b). It is important to note that this is already close to the size of the final copper particles (typically 5–15 nm). Therefore, a low degree of embedment of the resulting Cu surface and, thus, a large accessible Cu surface area can be expected. This step already pre-determines the meso-structure and porosity of the final $Cu/ZnO/Al_2O_3$ aggregates.

Second, the individual needles are decomposed into nano-particles of the oxides, mostly CuO and ZnO, during calcination. Care has to be taken not to completely destroy the needle-like meso-structure and the porosity of the oxide intermediate by too severe calcination conditions. The maximum of the BJH pore size distribution for the calcined sample shown in Fig. 5 was found at 20 nm, which is indicative of the presence of inter-particle pores between fine CuO and ZnO particles.

Both steps are prerequisite for the formation of porous aggregates with alternating arrangement of Cu and ZnO nanoparticles after activation, which can be seen as the target microstructure of commercial $Cu/ZnO/Al_2O_3$ methanol synthesis catalysts [23] (Fig. 5d). The effectiveness of the latter process is mostly determined by the Cu:Zn ratio in the zinican malachite precursor phase, which depends mainly on the nominal composition of the starting solutions, but also on the exact parameters during precipitation and ageing such as pH, temperature and mode of addition. For example, it is shown in Ref. [15] that, if a decreasing pH co-precipitation is used instead of working at constant pH, the critical limit of Zn^{2+} incorporation into zincian malachite is only 11%. The final pH after addition of the acidic metal solution into the soda receiver solution was near pH 9 in this case, instead of pH 7 for the constant pH process. The meso-structuring step will be additionally governed, e.g. by stirring and ionic strengths, which influence the dissolution/re-precipitation chemistry during the important ageing step.

All these determinants, which affect the phase formation during ageing, form a multi-dimensional parameter space and their com-

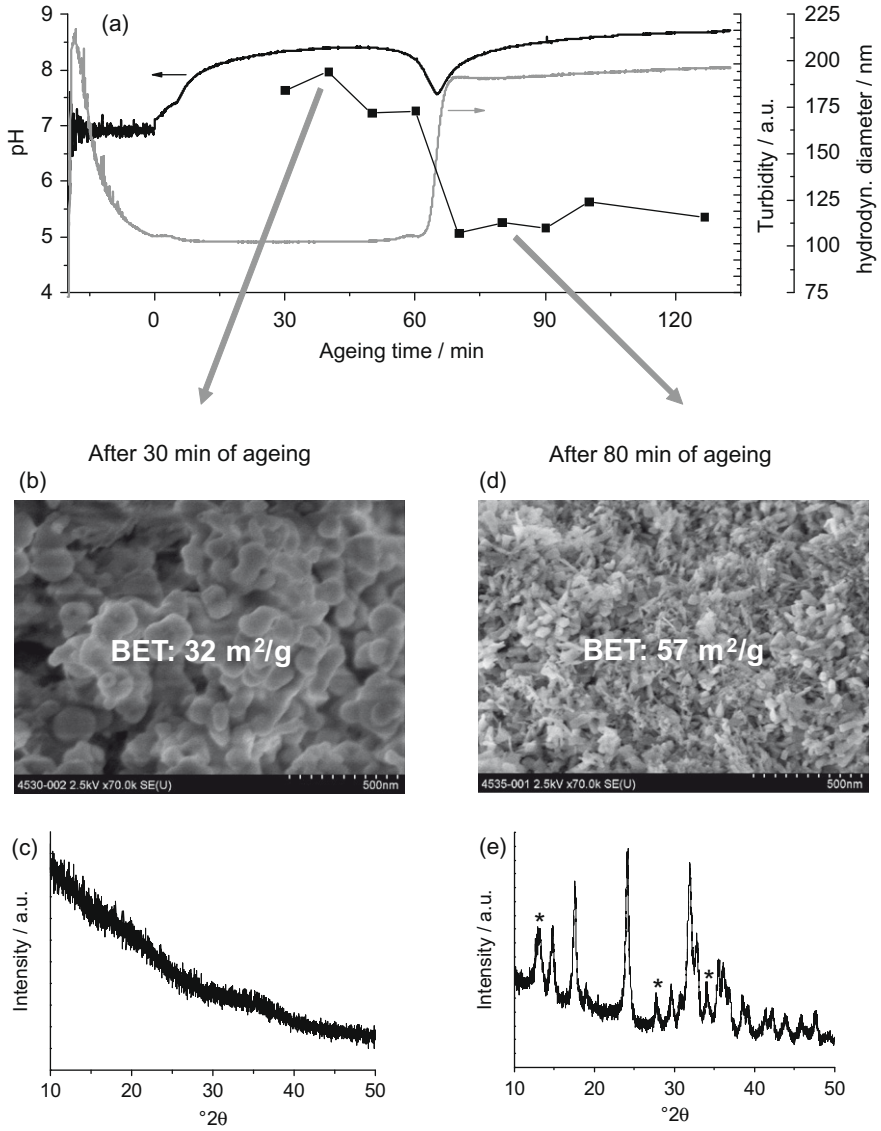

Fig. 4. Evolution of pH (black curve), turbidity (grey curve) and hydrodynamic particle diameter (symbols) during co-precipitation and ageing of a Cu,Zn (70:30) precursor (a). Specific surface area, SEM micrograph (b, d) and XRD pattern (c, e) of the precipitate after 30 and 80 min of ageing. The well-resolved peaks of aurichalcite are marked in (e), all other reflections are due to zinician malachite or to an overlap of peaks from both phases.

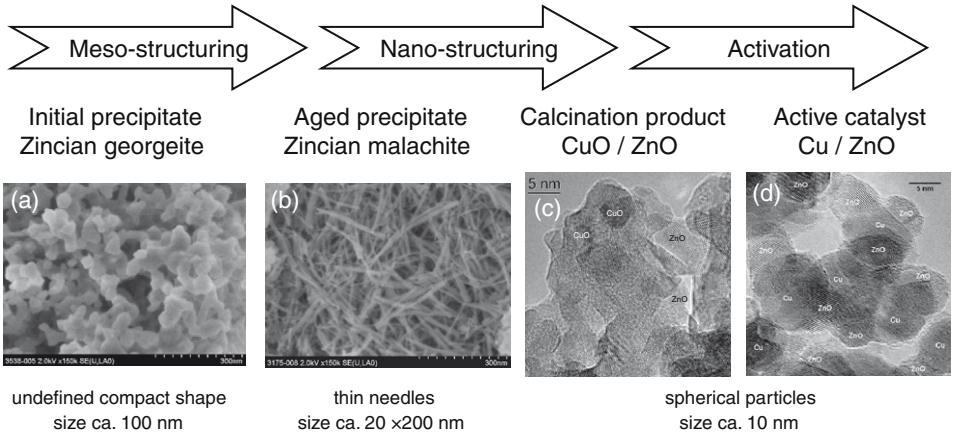

Fig. 5. Electron microscopy images of the materials obtained at different stages in the course of the preparation of $Cu/ZnO/Al_2O_3$ catalysts.

plex interplay is the basis for the so-called chemical memory of $Cu/ZnO/(Al_2O_3)$ catalysts. Parameters, which favor the discussed meso- and nano-structuring processes, have been determined empirically and resulted in the technically applied synthesis route

for $Cu/ZnO/Al_2O_3$ catalysts. For instance, the optimal setting for acidity and temperature is $6 < pH < 7$ and $60 < T < 70$, which was recently confirmed in a comprehensive parallel preparation and testing study by Baltes et al. [7].

The model of subsequent meso- and nano-structuring of zincian malachite provides the basis for two rational approaches for further optimization of the Cu/ZnO system. Either, a higher level of Zn incorporation into the properly meso-structured zincian malachite phase should be targeted or the meso-structuring of precursor phases exhibiting already a lower Cu:Zn ratio, preferably near 1:1, should be optimized. The former approach aims at further optimization of the conventional process by finding conditions of precipitation and ageing, which lead to a shift of the critical composition beyond 28% Zn, i.e. in the regime of natural rosasite [15]. Rosasite is a mineral of the same general composition as zincian malachite and has a closely related crystal structure, but it occurs with Zn contents of up to 50%. Combined with the meso-structure of synthetic zincian malachite, i.e. in form of small needles, such material can be seen as an ideal catalyst precursor.

Possible precursor phases for the latter approach are aurichalcite, but also amorphous basic carbonates or hydrotalcite-like phases, which present fewer limitations of composition and can accommodate Cu:Zn(+Al) ratios near unity. Investigations of mixed Cu, Zn, Al hydrotalcite-like materials, which will be reported elsewhere, showed that indeed very small Cu particles were formed after calcination and reduction from such Cu-poorer precursors, but unfortunately – similar to the aurichalcite phase – the meso-structure was found to be unfavorable and embedment of the Cu clusters in a continuous oxide matrix was observed. Here, the goal should be to find conditions for direct co-precipitation of very small precursor particles with dimensions in the low nm range in order to suppress the burying of active Cu clusters in the final catalyst.

4. Conclusion

The active Cu surface area of Cu/ZnO catalysts is correlated with the degree of Zn incorporation into the zincian malachite precursor phase. On the basis of this relation, the industrially applied route of preparation can be rationalized: the nominal metal composition as well as synthesis parameters such as temperature and acidity were empirically chosen to maximize this critical Zn content. Highly active catalysts develop from this precursor phase by subsequent meso- and nano-structuring: First, zincian malachite is prepared by co-precipitation and ageing in the form of thin needles, arranged in a loose network, which already pre-determines the porosity of the final catalyst. Second, the individual needles are thermally decomposed into much smaller CuO and ZnO particles resulting in the unique microstructure of industrial catalysts with porous aggregates of alternating Cu and ZnO particles after activation.

Acknowledgments

This paper has emerged from the work in a joint research project "Next generation methanol synthesis catalysts" in cooperation with Süd-Chemie AG, Bruckmühl, Germany, Ruhr-University Bochum, Germany, and NanoC, Kuala Lumpur, Malaysia. The project was funded by the German Federal Ministry of Education and Research (BMBF, FKZ 01RI0529). Fruitful discussions in the framework of this project with Martin Muhler, Benjamin Kniep, Richard Fischer, Sharifah B. Abd Hamid, Annette Trunschke and Robert Schlögl are greatly acknowledged. Thanks are given to Eduard Fitz, Andreas Furche, Igor Kasatkin, Edith Kitzelmann, Gisela Lorenz and Gisela Weinberg for their help with sample characterizations. Robert Schlögl is gratefully acknowledged for his continuous support.

References

[1] K. Klier, Adv. Catal. 31 (1982) 243.
[2] G.C. Chinchen, P.J. Denny, D.G. Parker, G.D. Short, M.S. Spencer, K.C. Waugh, D.A. Whan, Prepr. Am. Chem. Soc. Div. Fuel Chem. 29 (1984) 178.
[3] D. Waller, D. Stirling, F.S. Stone, M.S. Spencer, Faraday Discuss. Chem. Soc. 87 (1989) 107.
[4] P. Porta, S. De Rossi, G. Ferraris, M. Lo Jacono, G. Minelli, G. Moretti, J. Catal. 109 (1988) 367.
[5] D.M. Whittle, A.A. Mirzaei, J.S.J. Hargreaves, R.W. Joyner, C.J. Kiely, S.H. Taylor, G.J. Hutchings, Phys. Chem. Chem. Phys. 4 (2002) 5915.
[6] C. Kiener, M. Kurtz, H. Wilmer, C. Hoffmann, H.-W. Schmidt, J.-D. Grunwaldt, M. Muhler, F. Schüth, J. Catal. 216 (2003) 110.
[7] C. Baltes, S. Vukojevic, F. Schüth, J. Catal. 258 (2008) 334.
[8] F.S. Stone, D. Waller, Top. Catal. 22 (2003) 305.
[9] B. Bems, M. Schur, A. Dassenoy, H. Junkes, D. Herein, R. Schlögl, Chem. Eur. J. 9 (2003) 2039.
[10] T. Fujitani, J. Nakamura, Catal. Lett. 56 (1998) 119.
[11] R.G. Herman, K. Klier, G.W. Simmons, B.P. Finn, J.B. Bulko, T.P. Kobylinski, J. Catal. 56 (1979) 437.
[12] G.C. Chinchen, C.M. Hay, H.D. Vanderwell, K.C. Waugh, J. Catal. 103 (1987) 79.
[13] O. Hinrichsen, T. Genger, M. Muhler, Chem. Eng. Technol. 23 (2000) 956.
[14] M.M. Günter, T. Ressler, B. Bems, C. Büscher, T. Genger, O. Hinrichsen, M. Muhler, R. Schlögl, Catal. Lett. 71 (2001) 37.
[15] M. Behrens, F. Girgsdies, A. Trunschke, R. Schlögl, Eur. J. Inorg. Chem. 10 (2009) 1347.
[16] F.S. Stone, D. Waller, Top. Catal. 22 (2003) 305.
[17] H. Wilmer, O. Hinrichsen, Catal. Lett. 82 (2002) 117.
[18] R. Naumann d'Alnoncourt, X. Xia, J. Strunk, E. Löffler, O. Hinrichsen, M. Muhler, Phys. Chem. Chem. Phys. 13 (2006) 1525.
[19] N.-Y. Topsøe, H. Topsøe, Top. Catal. 8 (1999) 267.
[20] J.D. Grunwaldt, A.M. Molenbroek, N.Y. Topsoe, H. Topsoe, B.S. Clausen, J. Catal. 194 (2000) 452.
[21] C.V. Ovesen, B.S. Clausen, J. Schiøtz, P. Stoltze, H. Topsøe, J.K. Nørskov, J. Catal. 168 (1997) 133.
[22] P.C.K. Vesborg, I. Chorkendorff, I. Knudsen, O. Balmes, J. Nerlov, A.M. Molenbroek, B.S. Clausen, S. Helveg, J. Catal. 262 (2009) 65.
[23] I. Kasatkin, P. Kurr, B. Kniep, A. Trunschke, R. Schlögl, Angew. Chem. 119 (2007) 7465.
[24] A.M. Pollard, M.S. Spencer, R.G. Thomas, P.A. Williams, J. Holt, J.R. Jennings, Appl. Catal. A 85 (1992) 1.
[25] B.L. Kniep, T. Ressler, A. Rabis, F. Girgsdies, M. Baenitz, F. Steglich, R. Schlögl, Angew. Chem., Int. Ed. 43 (2003) 112.